equiv)[10] followed by a solution of dry *tert*-butyl hydroperoxide in toluene (2 equiv) for 2 h at room temperature to give stereospecifically (by TLC and ^{1}H NMR analyses) (±)-ovalicin (**1**), which was isolated by chromatography on triethylamine-deactivated sg (3:1 hexane–ethyl acetate) in 89% yield. Synthetic (±)-**1** was indistinguishable from an authentic sample by ^{1}H NMR, IR, mass spectra, ^{13}C NMR analyses as well as chromatographic mobility on sg in several solvent systems.

The method outlined above for the synthesis of 1,4-dienes **6a** and **6b** represents a new approach to trisubstituted olefins which should be widely useful because it is simple, C–C connective, and stereospecific. It demonstrates a previously unrecognized property of the Shapiro reaction to produce the *E*-trisubstituted azenolate geometry which then can be translated into *E*-trisubstituted olefins such as **6**. The novel synthesis of epoxy ketone **5**, the highly stereoselective conversion of **5** to **7**, and the stereospecific, internally directed epoxidation of **13** to ovalicin are also noteworthy.[11]

Supplementary Material Available: Spectroscopic data (PMR, ^{13}C NMR, IR, and mass spectral) are provided for compounds **3–5**, **6b,c** **7–9**, α-bromo α′-methyl enol ether of **10**, **10–13**, and (±)-**1** (synthetic) (3 pages). Ordering information is given on any current masthead page.

(10) (a) Sharpless, K. B.; Michaelson, R. C. *J. Am. Chem. Soc.* **1973**, *95*, 6138. (b) Hill, J. G.; Rossiter, B. E., Sharpless, K. B. *J. Org. Chem.* **1983**, *48*, 3607.

(11) This research was supported by grants from the National Institutes of Health and the National Science Foundation. We are grateful to Drs. H. P. Sigg and P. Bollinger of the Sandoz Co., Basel, Switzerland for a sample of ovalicin.

Electronic Structure of the $MoFe_3S_4(SH)_6^{3-}$ Ion†

Michael Cook and Martin Karplus*

Department of Chemistry, Harvard University
Cambridge, Massachusetts 02138

Received June 18, 1984

Recently several single- and double-cube compounds containing the cubane-type $[MoFe_3S_4]^{3+}$ core cluster have been synthesized.[1-6] The single-cube $MoFe_3S_4$ cluster is of particular interest because of its possible relation to the FeMo cofactor of nitrogenase[1,4] and its structural similarity to the $[Fe_4S_4]^{2+}$ site of oxidized ferredoxins. In this paper we report results of MS–Xα calculations on the hypothetical $MoFe_3S_4(SH)_6^{3-}$ cluster, a 289-electron system, and compare them with experimental data and with the Fe_4S_4 cluster calculations of Aizman and Case.[7] Figure 1 illustrates the structure used in the calculations. In the Xα method, both spin-restricted (same spatial orbitals for α and β spin) and spin-unrestricted calculations (different spatial orbitals for different spins) can be performed. While the former are simpler to interpret in ligand-field terms, an unrestricted treatment generally yields more satisfactory results for open-shell systems; the calculations we report here are all spin unrestricted.

Single-cube $MoFe_3S_4$ clusters are found experimentally to have quartet spin ($S = {}^3/_2$).[4] In C_{3v} symmetry the lowest energy quartet Xα configuration (Figure 2) is $[\cdots(16e^{\alpha})^2(16e^{\beta})^2(4a_2{}^{\alpha})^1(17e^{\alpha})^2]$. This quartet is not, however, the Xα ground state. Two occupied

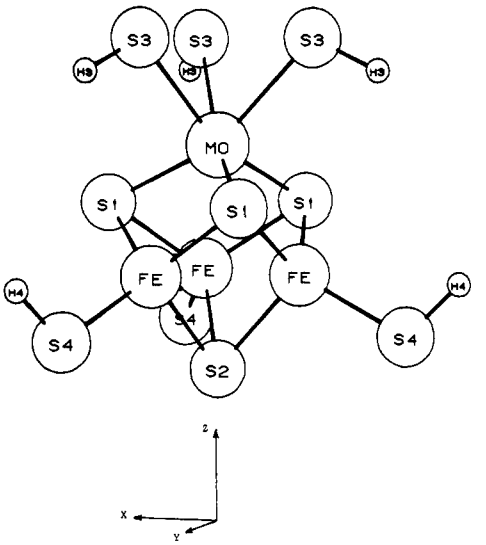

Figure 1. ORTEP drawing of the model $MoFe_3S_4(SH)_6^{3-}$ cluster. This C_{3v} model geometry is based on averaged interatomic distances and bond angles of the core from the crystal structure[6] of $Mo_2Fe_6S_8(SEt)_9^{3-}$; all the single- and double-cube clusters have very similar core geometries. The cartesian axes show the orientation of the molecule in the coordinate system. In units of a_0, the (x, z) coordinates of the atoms lying in the xz plane are as follows: Mo (0.0, 2.3619), Fe (-2.9316, -1.8670), S1 (4.0008, 0.4302), S2 (0.0, -5.0061), S3 (-3.3942, 5.8276), S4 (-6.6850, -3.7913), H3 (-5.6926, 4.7848), H4 (-8.5351, -2.0745). Out-of-plane atomic coordinates are related to these by ±120° rotations about the z axis.

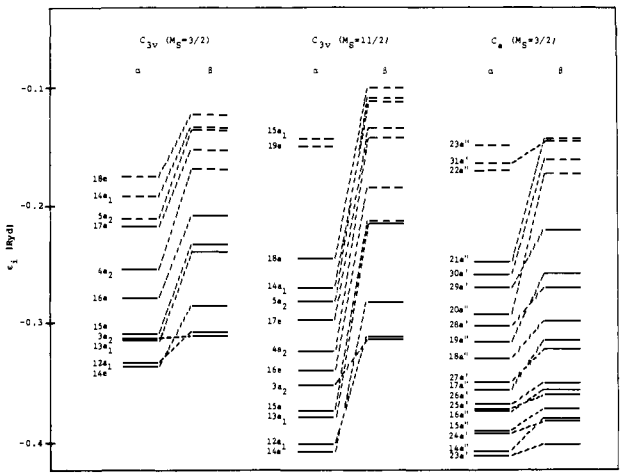

Figure 2. One-electron energy level diagrams for the different states of the $MoFe_3S_4(SH)_6^{3-}$ cluster; only the energy levels near the highest occupied orbital are shown. Occupied spin oribtals are denoted by solid horizontal lines, virtual levels by broken lines. Each α-spin orbital is connected to the corresponding β-spin level by a dashed line.

$16e^{\beta}$ spin orbitals (-0.207 Ry) lie above an unoccupied $5a_2{}^{\alpha}$ level (-0.209 Ry). Flipping the spin of one of the high-energy β electrons and transferring it to $5a_2{}^{\alpha}$ decreases the total energy, while lowering additional unoccupied α-spin levels below occupied β-spin levels. This self-reinforcing process continues until an $M_S = {}^{11}/_2$ state is reached in which all the occupied levels lie below the virtual levels (Figure 2). The configuration is $[\cdots(13a_1{}^{\alpha})^1(13a_1{}^{\beta})^1(15e^{\alpha})^2(16e^{\alpha})^2(4a_2{}^{\alpha})^1(17e^{\alpha})^2(5a_2{}^{\alpha})^1(14a_1{}^{\alpha})^1(18e^{\alpha})^2]$, and the state energy is 1.32 eV below that of the quartet.

This $M_S = {}^{11}/_2$ configuration is the Xα ground state in C_{3v} symmetry, but it is necessary to investigate whether a determinant of reduced symmetry can yield an even lower energy. Such spatial instabilities are well-known in Hartree–Fock[8-10] and Xα[11-14]

†Supported in part by a grant from the National Science Foundation.

(1) Holm, R. H. *Chem. Soc. Rev.* **1981**, *10*, 455.
(2) Armstrong, W. H.; Mascharak, P. K.; Holm, R. H. *J. Am. Chem. Soc.* **1982**, *104*, 4373.
(3) Mascharak, P. K.; Armstrong, W. H.; Mizobe, Y.; Holm, R. H. *J. Am. Chem. Soc.* **1983**, *105*, 475.
(4) Mascharak, P. K.; Papaefthymiou, G. C.; Armstrong, W. H.; Foner, S.; Frankel, R. B.; Holm, R. H. *Inorg. Chem.* **1983**, *22*, 2851.
(5) Palermo, R. B.; Singh, R.; Bashkin, J. R.; Holm, R. H. *J. Am. Chem. Soc.* **1984**, *106*, 2600.
(6) Wolff, T. E.; Berg, J. M.; Hodgson, K. O.; Frankel, R. B.; Holm, R. H. *J. Am. Chem. Soc.* **1979**, *101*, 4140.
(7) Aizman, A.; Case, D. A. *J. Am. Chem. Soc.* **1982**, *104*, 3269.
(8) Löwdin, P. O. *Rev. Mod. Phys.* **1963**, *35*, 496.
(9) Musher, J. I. *Chem. Phys. Lett.* **1970**, *7*, 397.
(10) Bénard, M.; Paldus, J. *J. Chem. Phys.* **1980**, *72*, 6546.
(11) Noodleman, L.; Norman, J. G., Jr. *J. Chem. Phys.* **1979**, *70*, 4903.

0002-7863/85/1507-0257$01.50/0

Table I. $MoFe_3S_4(SH)_6^{3-}$ One-Electron Properties

	net atomic charge and spin distributions[a]							
	metal		S*		S		H	
	Mo	Fe	S1	S2	S3	S4	H3	H4
total charge: *xz* plane	42.45	26.61	15.93	15.84	16.63	16.36	0.70	0.66
out-of-plane		26.65	15.91		16.63	16.36	0.70	0.66
$\alpha-\beta$ density: *xz* plane	−0.39	−3.07	0.06	0.04	0.03	−0.11		−0.01
out-of-plane		3.06			0.03	0.12		0.01

	quadrupole splittings and isomer shifts	
	Xα	exptl[b]
β-Fe		
ΔE_Q, mm/s[c]	1.395	1.60
η	0.94	
δ, mm/s	0.24	0.30
sign of principal component	(−)	(−)
α-Fe		
ΔE_Q, mm/s[c]	1.396	1.18
η	0.27	
δ, mm/s	0.30	0.30
sign of principal component	(−)	(−)

[a] In units of number of electrons. The atomic charge and spin densities are calculated using the charge-partitioning method of Case and Karplus, including intersphere and outer-sphere charges.[15-17] [b] Reference 4. The experimental results are for $MoFe_3S_4(S\text{-}p\text{-}C_6H_4Cl)_4((al)_2cat)^{3-}$. [c] Assuming $Q_{Fe}(1-R) = 0.143b$, e^2qQ/h (mm/s) = 2.8907q (au), and $\Delta E_Q = 1/2\ e^2Q/h\ (1+\eta^2/3)^{1/2}|q_{principal}|$. The electronic charge densities δ_{el} (au) at the Fe nuclei have been converted to isomer shifts δ (mm/s) using a linear relationship which fits δ_{el} from MS-Xα calculations on the 1-Fe clusters $Fe(SH)_4^{1-,2-}$ to the experimental isomer shifts of $Fe(S_2\text{-}o\text{-}xyl)_2^{1-,2-}$; the relationship is δ (mm/s) = 0.579[11 877.765 − δ_{el} (au)] + 0.13.

theory; they are particularly common in systems where transition-metal ions are weakly coupled. In the $MoFe_3S_4$ cluster we find a low-energy broken-symmetry solution on descent to the C_s subgroup, where only the *xz* plane in Figure 1 remains a symmetry operation. The C_s ground configuration (Figure 2) is $[\cdots(20a''^{\alpha})^1(29a'^{\alpha})^1(29a'^{\beta})^1(30a'^{\alpha})^1(21a''^{\alpha})^1]$; it lies 0.84 eV below the $M_S = {}^{11}/_2$, C_{3v} wavefunction and has quartet spin, in agreement with experiment on clusters of actual C_s symmetry.[4]

As is usual in theoretical calculations, the metal atoms are found to be nearly neutral (Table I). There is little difference of net charge between the two inequivalent iron sites. The spin-coupling scheme of the $MoFe_3S_4$ cluster is very similar to that of the Fe_4S_4 cluster.[7] In $Fe_4S_4(SH)_4^{2-}$, there are formally two Fe^{2+} and two Fe^{3+} irons; in the lowest energy broken-symmetry solution these form two ferromagnetic Fe^{2+}–Fe^{3+} pairs with antiferromagnetic coupling between pairs. In $MoFe_3S_4(SH)_6^{3-}$ we also have a Fe–Fe pair, coupled antiferromagnetically to a Fe–Mo pair (Table I). The iron in the C_s plane, coupled to Mo, is distinct from the other two irons.

The magnitude of the net spin on β-Fe (*xz*-plane iron) and each of the α-Fe atoms (out-of-plane irons) are nearly equal, despite their different spin couplings. Assuming $MoFe_3S_4$ formal charges of two Fe^{3+}, Fe^{2+}, and Mo^{3+}, the iron spin density of ±3.06 is ~65% of that for an isolated $Fe^{2.67+}$ ion. This is consistent with the Fe_4S_4 results,[7] in which the irons also carry 65% of the spin implied by their formal charges. By contrast, Mo has a net spin of only -0.4, ~13% of the value for an isolated Mo^{3+} ion. In a spin-restricted calculation the metal spin densities would be due entirely to the singly occupied molecular orbitals at the top of the valence band, but the spin-unrestricted treatment shows that the dominant contribution arises from the different spatial distributions of the α- and β-spin components of the doubly occupied molecular orbitals. In the $MoFe_3S_4$ cluster the three singly occupied levels produce spin densities of 0.33, 0.47, and 0.41 on Mo, α-Fe, and β-Fe, respectively. The difference between these values and the net spin densities of -0.39, 3.06, and -3.07 is due to the contribution from doubly occupied orbitals.

The highest occupied spin orbitals of the Fe_4S_4 cluster are two mirror-image metal levels, each localized on one of the Fe^{2+}–Fe^{3+} pairs and having opposite spin to the net spin density of the pair.[7] These can be thought of as adding a fraction of a sixth 3d electron to the high-spin metal atoms. These two Fe_4S_4 levels have close counterparts in the $MoFe_3S_4$ cluster; $29a'^{\beta}$ is localized on the two α-Fe atoms while $30a'^{\alpha}$ is concentrated on Mo and β-Fe. For both orbitals the interaction between the metal d functions is net bonding, as in the corresponding Fe_4S_4 orbitals. There are two additional occupied metal levels in the $MoFe_3S_4$ cluster which have no counterparts in the Fe_4S_4 cluster; $19a''^{\beta}$ and $28a'^{\beta}$ are localized on Mo and the two α-Fe atoms, with net d-orbital bonding between Mo and the two α-Fe's. In $28a'^{\beta}$ there is constructive overlap between the αFe atoms, while in $19a''^{\beta}$ a nodal plane separates the two.

The "metal-localized" levels considered above have more than 75% of their charge density on metal. The other occupied orbitals at the top of the valence band in the $MoFe_3S_4$ cluster, as in the Fe_4S_4 cluster, are delocalized over both metal and sulfur with less than ~50% metal character, except for $29a'^{\alpha}$, which has 67% metal character distributed among all four metal atoms. The generally delocalized nature of the upper orbitals found in these spin-unrestricted calculations is likely to be important in electron-transfer processes.

Some one-electron properties calculated from the broken-symmetry wavefunction are listed in Table I. The antiferromagnetic coupling shown by the spin-density distributions is consistent with the observed hyperfine fields at the iron nuclei, which are opposite in sign for the two unique iron sites.[4] The calculated isomer shifts and quadrupole splittings are in good agreement with Mössbauer results for a C_s single-cube cluster, and the signs of the principal components of the Fe quadrupole coupling tensors are correct. The Mössbauer spectrum of $MoFe_3S_4$ clusters is interpreted as an overlapping pair of doublets in an approximate 2:1 intensity ratio,[4] indicating that the iron in the C_s symmetry plane is physically distinct from the other two irons. In the Fe_4S_4 cluster, by contrast, the sites that appear distinct in the broken-symmetry subgroup are experimentally equivalent; in that case, the total molecular wavefunction is an equal combination of two broken-symmetry "resonance forms".[7] Although the calculated ΔE_Q for the two Fe sites in the $MoFe_3S_4$ cluster are essentially identical, there is a large difference in their anisotropies. It would be interesting to have single-crystal measurements of the quadrupole coupling tensors to test this result.

The oxidation–reduction properties of the $MoFe_3S_4$ clusters are important. Although we have not performed SCF calculations on the reduced $MoFe_3S_4$ cluster, inspection of Figure 2 suggests that on reduction the added electron enters the lowest majority-spin

(12) Noodleman, L. *J. Chem. Phys.* **1981**, *74*, 5737.
(13) Norman, J. G., Jr.; Ryan, P. B.; Noodleman, L. *J. Am. Chem. Soc.* **1980**, *102*, 4279.
(14) Noodleman, L.; Baerends, E. J. *J. Am. Chem. Soc.* **1984**, *106*, 2316.
(15) Case, D. A.; Karplus, M. *Chem. Phys. Lett.* **1976**, *39*, 33.
(16) Cook, M.; Karplus, M. *J. Chem. Phys.* **1980**, *72*, 7.
(17) Case, D. A.; Cook, M.; Karplus, M. *J. Chem. Phys.* **1980**, *73*, 3294.

level, $22a''^{\alpha}$ ($20a''^{\beta}$ lies at slightly lower energy in Figure 2, but an electron entering this minority-spin level would receive a much smaller exchange stabilization than one entering $22a''^{\alpha}$). Occupation of $22a''^{\alpha}$ would yield a quintet state, in agreement with the experimental result.[4] Since $22a''^{\alpha}$ is localized largely on Mo and β-Fe, occupation of this level should alter ΔE_Q primarily for the minority iron site, as is found experimentally.[4]

A more detailed analysis of the $MoFe_3S_4$ cluster and results of other studies on iron–sulfur and molybdenum–iron–sulfur clusters will be reported in future publications.

Acknowledgment. We thank Professor Richard Holm for many valuable discussions and helpful suggestions and for partial support of this research through NSF Grant CHE81-06017. We also thank Jeremy Berg, Jim Bashkin, and David Case for helpful disscusions.

$IrH_4(PMe_2Ph)_3^+$: Its Characteristic Reactivity and Use as a Catalyst for Isomerization of $IrH_3(PMe_2Ph)_3$

Larry F. Rhodes and Kenneth G. Caulton*

Department of Chemistry, Indiana University Bloomington, Indiana 47405

Received September 24, 1984

Our studies of the interaction of transition-metal polyhydrides with electrophiles and oxidants has succeeded in characterizing a variety of simple adducts as precursors to electron transfer or to H_2 elimination.[1-5] We have noted that binding of the electrophile Cu^+ to *fac*-IrH_3P_3 ($P \equiv PMe_2Ph$) gives an adduct which shows *no* interconversion with the Cu^+ adduct of *mer*-IrH_3P_3 at 25 °C (eq 1).

$$Cu(\textit{fac}\text{-}IrH_3P_3)_2^+ \not\rightleftharpoons Cu(\textit{mer}\text{-}IrH_3P_3)_2^+ \quad (1)$$

Thus, in spite of the apparent higher coordination number at iridium in these trimetal clusters, the iridium centers are stereochemically rigid.

Six-coordinate trihydride complexes are unique among polyhydrides in being stereochemically *rigid*. For example, *fac*- and *mer*-IrH_3P_3 do not isomerize in 2 days at 25 °C. Protonation of IrH_3P_3 isomers allows passage from the manifold of nonfluxional six-coordination isomers to the fluxional energy surface of coordination number 7. We report here on attempts to use this unique feature to selectively carry out an endergonic[6] isomerization of *fac*-IrH_3P_3.

The stoichiometric protonation of a CD_2Cl_2 solution of *fac*-IrH_3P_3 using 1 equiv of $HBF_4 \cdot Et_2O$ shows complete conversion (^1H and $^{31}P\{^1H\}$ NMR) to a single product.[7] Each resonance is a singlet, the implied equivalence of the phosphine ligands and of the hydride ligands being consistent with a fluxional seven-coordinate product formulated as $IrH_4P_3^+$. At -80 °C, the $^{31}P\{^1H\}$ NMR singlet splits into an AX_2 pattern, indicating that $IrH_4P_3^+$ has a pentagonal bipyramidal structure analogous to that of the isoelectronic molecule $OsH_4(PMe_2Ph)_3$[8] (see I). Curiously,

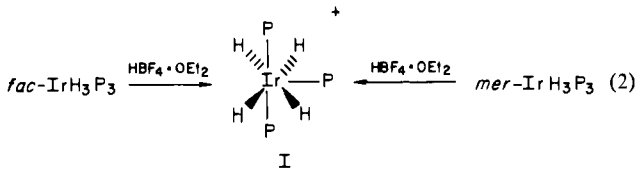

I

$IrH_4P_3^+$ exhibits no resolvable coupling of P to H in the ^1H NMR, even at −80 °C. The product of protonation of *mer*-IrH_3P_3 is identical (^1H and ^{31}P NMR) with that from *fac*-IrH_3P_3 (eq 2).

The following observations are consistent with H_2 elimination being a characteristic (but spectroscopically undetectable) reaction of $IrH_4P_3^+$ in dichloromethane: (1) stirring a CH_2Cl_2 solution of I at 25 °C under 150 psi of D_2 for 1 h resulted in complete conversion (^1H and ^2D NMR) to $IrD_4P_3^+$. (2) Sweeping a CH_2Cl_2 solution of $IrH_4P_3^+$ with N_2 for 20 min gives 80% conversion to *cis,mer*-$IrH_2(N_2)P_3^+$;[9] conversely, $IrH_4P_3^+$ is regenerated upon sweeping H_2 through the solution after an N_2 purge. (3) Several other ligands L (CO,[9] MeCN[9]) also yield *cis,mer*-$IrH_2LP_3^+$ when they are added to $IrH_4P_3^+$ in CH_2Cl_2 (eq 3). Even a ligand as

$$IrH_4P_3^+ \rightleftharpoons IrH_2P_3^+ + H_2 \xrightarrow{L} \textit{cis,mer}\text{-}IrH_2LP_3^+ \quad (3)$$

weak as THF will trap the unsaturated transient $IrH_2P_3^+$ when $IrH_4P_3^+$ is produced from *fac*-IrH_3P_3 and $HBF_4 \cdot OEt_2$ in THF as solvent.[9] This kinetically significant (even if endergonic[6]) reductive elimination (Ir(V) → Ir(III)) of H_2 is analogous to the same reaction that has been postulated[10] for $RuH_4(PPh_3)_3$, isoelectronic with $IrH_4P_3^+$. This ready loss of cis hydride ligands as H_2 from pentagonal-bipyramidal d^4 species is intriguing since the valence-isoelectronic $M(CO)_3(PR_3)_2H_2$ species (M = Mo, W; R = cyclohexyl and *i*-Pr) is now known to contain coordinated (η^2) dihydrogen.[11]

The *de*protonation of I using NEt_3 in CH_2Cl_2 was carried out and analyzed ($^{31}P\{^1H\}$ NMR) at -80 °C. By use of excess NEt_3, $IrH_4P_3^+$ is converted quantitatively to *mer*-IrH_3P_3. This isomer, obviously the kinetic product, has a planar T-shaped IrP_3 framework also present in $IrH_4P_3^+$ and thus is an obvious "least motion" product from removal of a proton from either inequivalent site in I. Since $IrH_4P_3^+$ is produced from *fac*-IrH_3P_3, the protonation/deprotonation sequence represents an acid-promoted stereoselective isomerization of *fac*- to *mer*-IrH_3P_3 which may be effected at −80 °C (eq 4).[12] Thermal equilibrium favors *fac* over *mer* in CH_2Cl_2 (see below).

$$\textit{fac}\text{-}IrH_3P_3 \xrightarrow{H^+} IrH_4P_3^+ \xrightarrow{NEt_3} \textit{mer}\text{-}IrH_3P_3 \quad (4)$$

The use of stoichiometric acid in a two-step procedure to catalyze isomerization of *mer*- and *fac*-IrH_3P_3 may be simplified by employing a substoichiometric amount of acid. Such an experiment is in fact a variant on the NEt_3 deprotonation described above, except that one of the isomers of IrH_3P_3 is now the attacking base. In practice, addition of 0.1 molar equiv of $HBF_4 \cdot OEt_2$ to *fac*-IrH_3P_3 in CD_2Cl_2 at 25 °C, followed by ^1H NMR (25 °C) measurement within 10 min, revealed an 88:12 mixture of *fac* and *mer* isomers (in addition to $IrH_4P_3^+$). When the experiment and analytical procedure are repeated beginning with *mer*-IrH_3P_3, the same 88:12 *fac/mer* equilibrium is reached. Finally, if 1:10 $HBF_4 \cdot OEt_2$ and *fac*-IrH_3P_3 are combined at −80 °C in CH_2Cl_2, catalyzed isomerization reaches equilibrium within 2 h at −80 °C, and an 88:12 ratio of *fac/mer* is again achieved. The fact that these isomerizations with substoichiometric quantities of acid do not function to give only *mer* is of course determined by thermodynamics; in the stoichiometric procedure with NEt_3

(1) Rhodes, L. F.; Zubkowski, J. D.; Folting, K.; Huffman, J. C.; Caulton, K. G. *Inorg. Chem.* **1982**, *21*, 4185.
(2) Rhodes, L. F.; Huffman, J. C.; Caulton, K. G. *J. Am. Chem. Soc.* **1983**, *105*, 5137.
(3) Bruno, J. W.; Huffman, J. C.; Caulton, K. G. *J. Am. Chem. Soc.* **1984**, *106*, 1663.
(4) Bruno, J. W.; Huffman, J. C.; Caulton, K. G. *J. Am. Chem. Soc.* **1984**, *106*, 444.
(5) Rhodes, L. F.; Huffman, J. C.; Caulton, K. G. *J. Am. Chem. Soc.* **1984**, *106*, 6874.
(6) I.e., $\Delta G > 0$.
(7) ^1H NMR (360 MHz, 25 °C in CD_2Cl_2) δ 7.50 (m, 9 H), 7.30 (m, 6 H), 1.71 (br s, 18 H), −8.39 (br s, 4 H). $^{31}P\{^1H\}$ (40.5 MHz, 25 °C in CD_2Cl_2) δ −37.55 (br s); (40.5 MHz, −80 °C in CD_2Cl_2) δ −41.59 (t, 1 P), −33.14 (d, 2 P, J = 18.5 Hz). At −80 °C, the hydride coupled ^{31}P NMR spectrum shows broadening in the −41.59 ppm resonance, due to unresolved coupling to hydride ligands.
(8) Hart, D. W.; Bau, R.; Koetzle, T. F. *J. Am. Chem. Soc.* **1977**, *99*, 7557.
(9) ^1H and ^{31}P NMR and IR data available as supplementary material.
(10) Knoth, W. H. *J. Am. Chem. Soc.* **1972**, *94*, 104.
(11) Kubas, G. J.; Ryan, R. R.; Swanson, B. I.; Vergamini, P. J.; Wasserman, H. J. *J. Am. Chem. Soc.* **1984**, *106*, 451.
(12) Deprotonation using NEt_3 at 25 °C is complicated by production of *cis,mer*-IrH_2ClP_3, from reaction with CH_2Cl_2 solvent. We attribute this to attack of solvent on $IrHP_3$, the Ir(I) product of deprotonation of the equilibrium concentration of $IrH_2P_3^+$. Compare: Harrod, J. F.; Yorke, W. J. *Inorg. Chem.* **1981**, *20*, 1156.

0002-7863/85/1507-0259$01.50/0